



Numerical study of the thermal performance and pressure drops of water-based Al_2O_3 - Cu hybrid nanofluids of different compositions in a microchannel heat sink

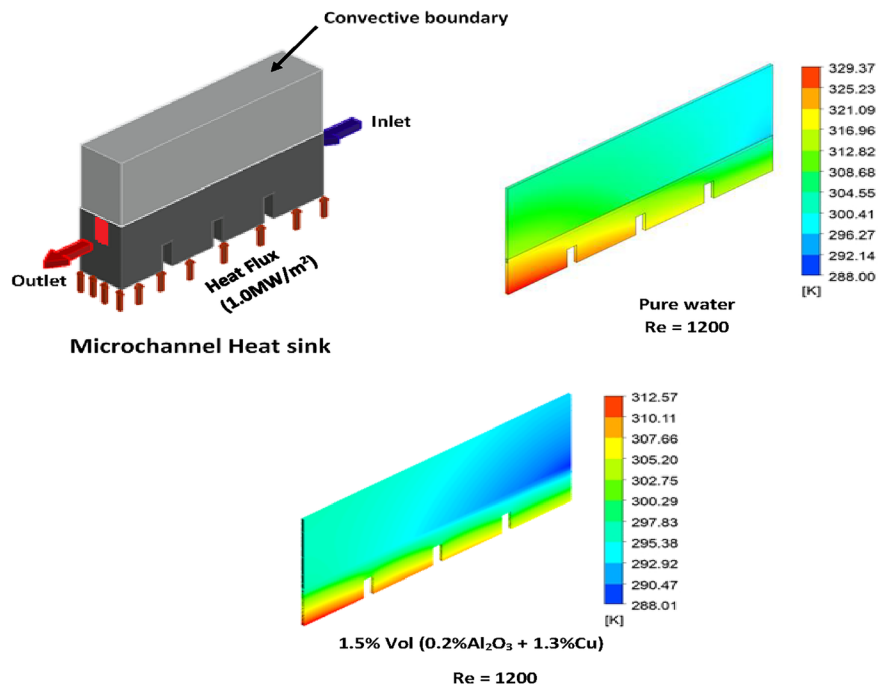
Oluwasegun S. Omosehin¹ · Adekunle O. Adelaja¹ · Olabode T. Olakoyejo¹ · Manasseh O. Oyekeye¹

Received: 19 October 2021 / Accepted: 9 May 2022 / Published online: 4 June 2022
© The Author(s), under exclusive licence to Springer-Verlag GmbH Germany, part of Springer Nature 2022

Abstract

This paper numerically investigates the effects of hybridization of water-based copper-alumina nanofluid on the thermal performance, pressure drop, and the figure of merit (FOM) inside a three-dimensional microchannel heat sink. The heat sink comprises a copper block with the top covered by a polycarbonate plastic (Lexan) to form a closed microchannel. A constant heat flux of 1.0 MW/m^2 is applied at the base of the heat sink. The Reynolds number is varied between 400 and 1200 for different volume concentrations of alumina and copper nanoparticles of 0.5–3.0% vol. Simulation in ANSYS Fluent is performed with a two-phase Eulerian-Eulerian model using the finite volume approach to solve the conjugate heat transfer problem. Experimental validations of the numerical models are in very good agreement. Furthermore, the result shows that the higher the relative concentration of copper nanoparticles, the better the thermal enhancement and FOM of the hybridized nanofluid. For design and operational conditions, the maximum FOM favour the concentration of copper nanoparticle $\geq 0.75\%$ for Re of 400 and $< 0.75\%$ vol. for Re of 1200.

Graphical abstract



Keywords Hybrid nanofluid · Thermal performance · Pressure drop · Microchannel · Heat sink

Extended author information available on the last page of the article

List of symbols

A	Area (m^2)
C_d	Drag co-efficient (-)
C_p	Specific heat capacity(J/kgK)
D_h	Hydraulic diameter (m)
d	Diameter (m)
F_d	Drag force (Pa/m)
F_{VM}	Virtual mass (Pa/m)
F_{col}	Particle –particle interaction force (Pa/m)
H_{ch}	Channel height (μm)
$h_{p,1}$	Fluid –particle heat transfer co efficient (W/m^2K)
K	Thermal conductivity ($W/m.K$)
L	Length (m)
Nu	Nusselt number (-)
P	Pressure (Pa)
q''	Heat flux (W/m^2)
Q_h	Volumetric rate of energy transfer (J/m^3s)
R_{th}	Thermal resistance(K/W)
Re	Reynolds number (-)
T	Temperature (K)
\vec{V}	Velocity vector (m/s)
W_{ch}	Channel width (μm)

Greek symbols

Δ	Difference
ρ	Density (kg/m^3)
α	Volume fraction (-)
μ	Dynamic viscosity ($kg/m s$)
β	Friction coefficient ($kg/m^3 s$)
Φ	Form factor

Subscripts

avg	Average
b	Base
B	Bulk
I	Inlet
P	Particle
S	Solid
f	Fluid
w	Wall
1	Primary phase (pure water)
2	Secondary phase (Alunima particles)
3	Secondary phase (copper particles)

1 Introduction

Conventional fluids such as water, oils, refrigerants, and glycol, are used in heat exchange systems—power plants, refrigeration, air conditioning systems, chemical and thermal processes, electronics, etc. However, their applications are becoming limited due to the current drive to design compact energy technologies with reduced weight and size and increased efficiency. In addition, aerospace, very

high-temperature applications, and continued advancement in technology increase heat flux and the need to remove enormous heat energy. The electronic industry is particularly faced with challenges relating to the cooling of devices for better performance. Since conventional fluids will not give an adequate and efficient technological solution, there is the need to take advantage of nanofluids because of the increased thermal performance and enhancement and lower pressure penalty.

In the last few decades, several studies have been conducted on the properties of various nanofluids, thermal performance, and pressure drops in heat exchangers of macro, mini and micro scales. The focus of this current study will be limited to the application of hybrid nanofluids in microchannels. Numerous literatures have been reviewed on this subject by notable researchers in this regard (Al Shdaifat et al. 2020; Alihosseini et al. 2020; Rajiv and Sokhal 2020). Just a few related studies will be reviewed in this study.

After many years of research on the type of working fluid used to achieve optimal performance of the microchannels, nanofluids have shown better heat transfer abilities. These nanofluids are the colloidal solution of nanometer-sized particles called nanoparticles. The improvements in the thermal performance are due to the relative movement between the base fluid and the suspended nanoparticles (Pinto and Fiorelli 2016). The common types of base fluid used are water, oil and lubricant, bio-fluids, organic fluids (refrigerants, triethylene-glycols), and other conventional fluids. Different nanoparticles include carbon-based nanoparticles (graphite, carbon nanotubes, diamonds), ceramic nanoparticles (Oxides of Aluminium and copper), stable metal nanoparticles (copper, gold), and functionalized nanoparticles (Sarkar 2011). Oxide nanoparticles have been most adopted in electronic cooling. The resulting nanofluids from suspended nanoparticles can be divided into mono-nanofluids (same particles) and hybrid nanofluids (dissimilar and composites nanoparticles). A study on single-phase, steady, laminar conjugate heat transfer in a microchannel was carried out by Yildizeli and Cadirci (2020) with ANSYS Fluent. A multi-objective optimization was conducted on the microchannel heat sink through a generic algorithm coded in MATLAB. The design variables included the channel width and channel height for the cross-section of the geometry, while the inlet Reynolds number was selected for the flow rate. They concluded that the optimal microchannel height ranged between 0.50 and 0.67 mm. Some researchers have investigated the thermophysical and rheological properties of mono and hybrid nanofluids (Suresh et al. 2011; Madhesh et al. 2014; Ambreen and Kim 2017; Madalina et al. 2018).

Water and Al_2O_3 /water nanofluid were employed by Kumar and Kumar (2020) as a coolant in six circular channel heat

sinks for an electronic chip to investigate the heat transfer rate, surface temperature, power consumption, thermal resistance, Nusselt number, and reliability of the microchannel heat sinks. They reported that the use of nanofluid increased the reliability, the Reynolds number, and decreased surface temperature, thermal resistance, and power consumption of the electronic chip. Hybrid nanofluids are produced by dispersing dissimilar nanoparticles in a complex state or mixture form. The main reason for hybrid nanofluids is to enhance the heat exchange rate and improve other specific attributes. Qu and Mudawar (2002) investigated experimentally and numerically both pressure drop and thermal performance of flow in a microchannel heat sink. A single-phase flow with deionized water as the cooling fluid and two heat flux levels of 100 and 200 W/cm² were considered. The conjugate heat transfer problem was also analyzed numerically to account for the temperature distribution. Heat transfer characteristics at the microchannel bottom wall, sidewalls, and the top wall were investigated. They noted that the very low thermal conductivity of the plastic cover of the microchannel results in the adiabatic nature at the top wall surface. The high value of heat flux and Nusselt number were recorded near the entrance for both the bottom wall and sidewall of the microchannel. An experimental and numerical investigation of the heat transfer and pressure drop of Al₂O₃/TiO₂ hybrid nanofluid was done by Kumar and Sarkar (2019). They noted that the two-phase mixture model accurately predicted the experimental data than the single-phase homogeneous approach. Al₂O₃ (10:0) hybrid nanofluid gave a thermal enhancement of 8.5% numerically and 12.8% experimentally. The pressure drop and friction factor rose as the volume fraction rose, but the temperature decreased. Kumar and Sarkar (2020) experimentally analyzed the hydrodynamic characteristics of a mini channel heat sink by considering different hybrid nanofluids. The different nanoparticle mixtures considered in the study included oxides-oxides, oxides-carbides, oxides-nitrides, oxides-carbon nanotubes, and oxides-metals. It was reported that there was an enhancement in the heat transfer characteristics for all hybrid nanofluids. However, Al₂O₃-MWCNT hybrid nanofluid exhibited the maximum enhancement and heat transfer effectiveness while Al₂O₃-AlN hybrid nanofluid had the maximum $h/\Delta P$ ratio. The maximum FOM was obtained for the nanofluids at the Reynolds number 345. Ataei et al. (2020) experimentally investigated the heat transfer and flow characteristics of hybrid Al₂O₃/TiO₂-water nanofluid in a mini channel heat sink with a hydraulic diameter of 2.0 mm. Constant heat flux boundary with 36 W was imposed at the bottom of the heat sink, and the Reynolds number varied between 400 and 1000 for nanofluid of volume fraction of 0.5%. A convective heat transfer coefficient and pressure drop augmentations of 16.97 and 29.54%, respectively, were obtained. Other studies on

the effect of various parameters on the thermal and hydraulic characteristics of mono and hybrid nanofluids have been considered (Minea 2020; Selvakumar and Suresh 2012; Suresh et al. 2012; Snoussi et al. 2018; Shkara et al. 2013; Labib et al. 2013).

On the two-phase modeling approach, Nimmagadda and Venkatasubbaiah (2017) investigated microchannel heat sink performance using pure water, hybrid nanofluid, and fluid hybridization. A two-phase mixture model that accounts for the conjugate heat transfer between the solid and fluid regions was developed to numerically estimate the heat transfer characteristic. The flow and thermal characteristics of pure water, aluminum (Al), copper (Cu), single-walled carbon nanotube, and hybrid nanofluid (Al + Cu, water + methanol) at various Reynolds numbers and nanoparticle volume concentrations were studied. It was reported that there was a pronounced improvement in the average Nusselt number for both the pure nanofluids and the hybrid nanofluids. Kalteh et al. (2011) numerically analyzed a laminar convective heat transfer of Cu/water nanofluid flowing inside an isothermally heated microchannel. An Eulerian two-phase model was adopted to simulate the flow and heat transfer characteristics. An insignificant relative velocity and temperature between the phases were observed. In another study, Kalteh et al. (2012) experimentally and numerically investigated a steady laminar convective heat transfer in a wide microchannel with alumina-water nanofluid as the cooling liquid. A single-phase homogeneous model and two-phase Eulerian-Eulerian approach were adopted. When compared, the two-phase flow result was observed to better agree with the experiment. Therefore, it was concluded that the two-phase flow modeling approach was more appropriate to analyse the nanofluid flow in the microchannel heat sink. Fard et al. (2010) reported that the average deviation between the experiment and the single-phase model was 16%, while for the two phases, methods it was 8%. Ghasemi et al. (2017), in their study on the significance of CuO nanoparticles in pure water on heat dissipation from the electronic components, noted that the result of the two-phase approach was better than the homogeneous.

From the literature, different authors have successfully employed the mixture model theory to investigate the heat transfer characteristics of hybrid nanofluid in microchannels. To the best of the authors' knowledge, limited numerical studies used ANSYS Fluent (two-phase Eulerian-Eulerian approach) to study the thermal and pressure drop characteristics of hybrid nanofluid in a microchannel. Therefore, there is a need for more studies to understand hybrid nanofluids and the expansion of the numerical database. Most importantly, this paper emphasizes that the FOM gives better information for the operation and design of the microchannel heat sink.

2 Geometry description

The schematic diagram of a narrow microchannel unit-cell heat sink with the critical dimensions (Table 1) is shown in Fig. 1. It consists of both the fluid and solid computational regions. The lower part of the heat sink is made of copper block covered with polycarbonate plastic (Lexan). Three 1.6 mm slots of height (H) are cut through the height of the copper block in order to provide a uniform heat flux distribution. The polycarbonate plastic cover and the copper block are treated as the computational solid region, while the fluid particle in the channel is treated as the computational fluid region. The hybrid nanofluid flows in the direction of the arrows through the channel.

3 Governing equation

The present problem is a laminar, steady-state, incompressible, and three-dimensional Eulerian-Eulerian two-phase flow. The solid and base fluid (pure water) have constant thermal properties except for viscosity, which varies with temperature. The geometric model consists of the primary phase (pure water) and two secondary phases (alumina and copper particles) with properties presented in Table 2. The conservation equations in Eulerian notation are as follows:

3.1 Mass conservation equation

The mass conservation equation of the base fluid and nanoparticles are presented in Eqs. (1–3)

Primary phase (pure water)

$$\nabla \cdot (\rho_1 \alpha_1 \vec{V}_1) = 0 \tag{1}$$

where ρ_1, α_1 and \vec{V}_1 are the density, volume concentration, and velocity vector of the primary phase, respectively.

Secondary phase (alumina particles)

$$\nabla \cdot (\rho_2 \alpha_2 \vec{V}_2) = 0 \tag{2}$$

where ρ_2, α_2 and \vec{V}_2 are the density, volume concentration, and velocity vector of the secondary phase (alumina particle), respectively.

Secondary phase (copper particles)

$$\nabla \cdot (\rho_3 \alpha_3 \vec{V}_3) = 0 \tag{3}$$

where ρ_3, α_3 and \vec{V}_3 are the density, volume concentration, and velocity vector of the secondary phase (Copper particles), respectively

$$\alpha_1 + \alpha_2 + \alpha_3 = 1 \tag{4}$$

3.2 Momentum conservation equation

The momentum conservation equation of the base fluid and nanoparticles are presented in Eqs. (5–7)

Primary phase (pure water)

$$\nabla \cdot (\rho_1 \alpha_1 \vec{V}_1 \vec{V}_1) = -\alpha_1 \nabla P + \nabla \cdot [\alpha_1 \mu_1 (\nabla \vec{V}_1 + \nabla \vec{V}_1^T)] + F_d + F_{VM} \tag{5}$$

Secondary phase (alumina particles)

$$\nabla \cdot (\rho_2 \alpha_2 \vec{V}_2 \vec{V}_2) = -\alpha_2 \nabla P + \nabla \cdot [\alpha_2 \mu_2 (\nabla \vec{V}_2 + \nabla \vec{V}_2^T)] - F_d - F_{VM} + F_{col} \tag{6}$$

Secondary phase (copper particles)

$$\nabla \cdot (\rho_3 \alpha_3 \vec{V}_3 \vec{V}_3) = -\alpha_3 \nabla P + \nabla \cdot [\alpha_3 \mu_3 (\nabla \vec{V}_3 + \nabla \vec{V}_3^T)] - F_d - F_{VM} + F_{col} \tag{7}$$

where F_{VM}, F_d and F_{col} are the virtual mass, drag, and particle-to-particle interaction forces, respectively. However, according to Kalteh et al. (2011), the virtual mass and particle to particle interaction force have an insignificant effect on heat transfer characteristics (Nusselt number). Hence, only the drag force and convective heat transfer between the primary and secondary phases are considered. The particle-to-particle heat transfer is neglected, and the gravitational and the lift forces attributable to the small size of the particles are also ignored.

The drag force between the primary phase and each secondary phase (alumina and copper particle) is calculated as

$$F_d = -\beta(\vec{V}_1 - \vec{V}_p) \tag{8}$$

The drag coefficient by Wen and Yu (1966) and Rowe (1961) is given as.

Table 1 Geometry dimensions

H_L (μm)	H_{ch} (μm)	H_c (μm)	w (μm)	W_{ch} (μm)	W_w (μm)	L (μm)	H (μm)	L_1 (μm)	L_2 (μm)	L_3 (μm)	L_4 (μm)
12,700	713	5637	467	231	118	44.8	3175	5	11.588	11.588	11.588

Fig. 1 Schematic diagram of the heat sink

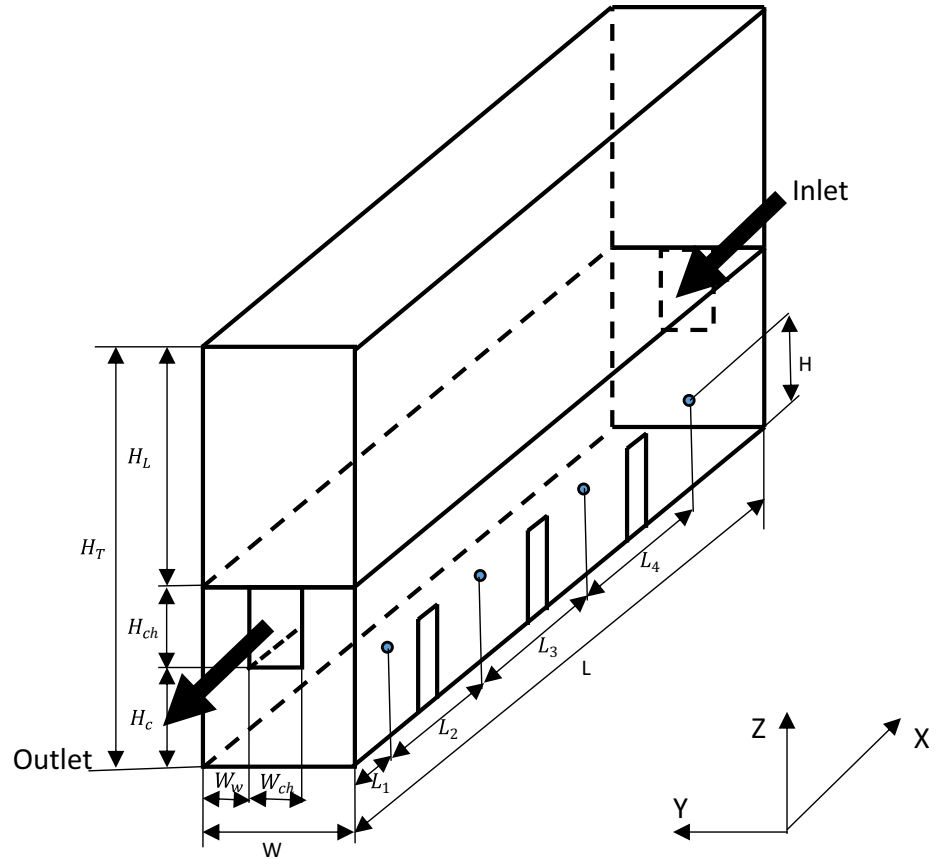


Table 2 Thermo-physical properties of pure water, copper and alumina particles

Materials	$\rho(\text{kg}/\text{m}^3)$	$C_p(\text{J}/\text{kg}\cdot\text{K})$	$k(\text{W}/\text{m}\cdot\text{K})$	$\mu(\text{kg}/\text{m}\cdot\text{s})$
Pure water	999.1	4184	0.5769	Temperature dependent
Alumina	3970	765	36	–
Copper particles	8933	385	400	–

$$\beta = \frac{3}{4} C_d \frac{\alpha_1 \alpha_p}{\varphi_p d_p} \rho_1 |\vec{V}_1 - \vec{V}_p| \alpha_1^{-2.65} \text{ Valid for two - phase flow } \alpha_1 > 0.8 \quad (9)$$

φ_p The form factor is considered as unity for a spherical particle.

$$C_d = \begin{cases} \frac{24}{Re_p} (1 + 0.15 Re_p^{0.687}) & Re_p < 1000 \\ 0.44 Re_p & Re_p \geq 1000 \end{cases} \quad (10)$$

where,

$$Re_p = \frac{\alpha_1 \rho_1 |\vec{V}_1 - \vec{V}_p| d_p}{\mu_1} \quad (11)$$

such that, \vec{V}_p, α_p and Re_p are equivalent to \vec{V}_2, α_2 and Re_2 for the secondary phase alumina particles.

\vec{V}_p, α_p and Re_p are equivalent to \vec{V}_3, α_3 and Re_3 for the secondary phase copper particles.

The particle diameter ($d_p = 40\text{nm}$) for both alumina and copper particles are equal.

3.3 The energy conservation equation

The energy conservation equation, neglecting the viscous dissipation and radiation, is thus given in Eqs. (12–14).

Primary phase (pure water)

$$\nabla \cdot (\rho_1 \alpha_1 C_{p1} T_1 \vec{V}_1) = \nabla \cdot (\alpha_1 K_1 \nabla T_1) - Q_h \quad (12)$$

Secondary phase (alumina particles)

$$\nabla \cdot (\rho_2 \alpha_2 C_{p2} T_2 \vec{V}_2) = \nabla \cdot (\alpha_2 K_2 \nabla T_2) + Q_h \quad (13)$$

Secondary phase (copper particles)

$$\nabla \cdot (\rho_3 \alpha_3 C_{p3} T_3 \vec{V}_3) = \nabla \cdot (\alpha_3 K_3 \nabla T_3) + Q_h \quad (14)$$

where Q_h is the volumetric rate of energy transfer between the primary and each secondary phase (alumina and copper particles), and it is expressed as

$$Q_h = h_{p,1} \frac{6\alpha_p}{d_p} (T_p - T_1) \tag{15}$$

Such that

$h_{p,1}$ and T_p are equivalent to $h_{2,1}$ and T_2 for secondary phase—alumina particles.

$h_{p,1}$ and T_p are equivalent to $h_{3,1}$ and T_3 for secondary phase—copper particles.

$h_{p,1}$ is the fluid–particle convective heat transfer coefficient, calculated based on the Gunn (1978) model.

3.4 The conservative energy equation for the solid wall domain

The heat conducted through the solid domain is expressed as

$$K_s \nabla^2 T_s = 0 \tag{16}$$

3.5 Governing boundary conditions

The base fluid and the particulate phase are allowed to enter the channel with a uniform axial velocity at a temperature of 15 °C, and the velocity is zero along all other solid boundaries (no-slip condition) (Nimmagadda and Venkatasubbaiah 2017; Shkarah et al. 2013). An outflow condition is considered at the outlet of the microchannel and the flow is assumed to be fully developed in order to compare the simulation with the existing experimental result. For the thermal boundary conditions, all the solid domain boundaries are considered adiabatic except for the bottom of the microchannel, which is subject to a constant heat flux of 1.0 MW/m². Convective heat transfer is assumed at the top of the channel with a heat transfer coefficient of 10 W/°C.m² at an ambient condition of 25 °C.

Mathematical expressions of the boundary conditions are listed below

Inlet condition

$$T_f = T_{in} = 15^\circ C \text{ for } x = 0, W_w \leq y \leq W_w + W_{ch} \text{ and } H_c \leq Z \leq H_c + H_{ch} \tag{17}$$

$$V_f = V_{in} \text{ (uniform axial velocity for both) (base fluid and particulate phase)} \tag{18}$$

Outlet conditions

An ambient outflow condition was applied at the outlet

$$\frac{\partial^2 T_f}{\partial X^2} = 0 \text{ for } x = L, W_w \leq y \leq W_w + W_{ch} \text{ and } H_c \leq Z \leq H_c + H_{ch} \tag{19}$$

Channel bottom (constant heat flux)

$$-k_s \frac{\partial T_s}{\partial Z} = q^{ii} \text{ for } 0 \leq x \leq L, 0 \leq y \leq W \text{ and } Z = 0 \tag{20}$$

Heat sink top surface (convective condition)

$$-k_s \frac{\partial T_s}{\partial Z} = h_c (T_s - T_\infty) \text{ for } 0 \leq x \leq L, 0 \leq y \leq W \text{ and } Z = H_T \tag{21}$$

where h_c is the convective heat transfer coefficient and T_∞ is the ambient temperature.

Interface condition

$$T_s = T_f \tag{22}$$

$$-k_s \frac{T_s}{\partial n} = -k_f \frac{T_f}{\partial n} \tag{23}$$

where n is the coordinate normal to the wall of the channel. k_f is the thermal conductivity of the fluid.

3.6 Pressure drop deduction

Pressure drop across the microchannel was calculated from the difference between the upstream and downstream pressure of the channel. The upstream and downstream pressures, p_{in} and p_{out} are the area-weighted average pressure at the inlet and outlet obtained from the numerical simulation using ANSYS—Postprocessor.

$$\text{Hence } \Delta p = p_{in} - p_{out} \tag{24}$$

where Δp is the pressure drop across the microchannel.

3.7 Average Nusselt number definition

The average Nusselt number (Nu_{avg}) of the flow field is dependent on the difference in temperature between the average wall temperature of the microchannel and the volume average (bulk) temperature of the mixture in the channel.

$$Nu_{avg} = \frac{q^w D_h}{k_f (T_w - T_B)} \tag{25}$$

q^w and D_h are the wall convective heat flux at the base area of the computational domain and hydraulic diameter of the microchannel. k_f is the thermal conductivity of the liquid as adopted by (Nimmagadda and Venkatasubbaiah 2017; Kalteh et al. 2012). However, in the Eulerian–Eulerian model, the mixture phase properties are calculated as the phase fraction weighted sum of the properties of each phase, that is:

Mixture thermal conductivity = (Volume fraction of primary phase x thermal conductivity of primary phase) + (Volume fraction of secondary phase x thermal conductivity of secondary phase).

T_w and T_B are the area-weighted average surface (wall) temperature of the microchannel and volume-weighted average temperature of the mixture obtained from the numerical simulation using the ANSYS- Postprocessor.

3.8 Thermal resistance

The thermal resistance of the microchannel is defined as

$$R_{th} = \frac{\Delta T}{q^{ii} A_b} \tag{26}$$

$$\Delta T = T_{max} - T_{in} \tag{27}$$

where A_b is the base area of the heat sink subjected to the heat flux, T_{max} is the maximum temperature at the base of the heat sink.

3.9 Error analysis

The experimental and numerical results are compared using the average deviation (AD) and mean average deviation (MAD) as expressed in Eqs. (28) and (29)

Average deviation (AD):

$$AD = \frac{1}{N} \sum_1^N \left[\frac{(\gamma_{pred} - \gamma_{exp}) \times 100\%}{\gamma_{exp}} \right] \tag{28}$$

Mean absolute deviation (MAD):

$$MAD = \frac{1}{N} \sum_1^N ABS \left[\frac{(\gamma_{pred} - \gamma_{exp}) \times 100\%}{\gamma_{exp}} \right] \tag{29}$$

where N is the number of data points, γ_{pred} and γ_{exp} are the experimental and predicted parameters such as temperature, Nusselt number, and pressure drop for which the errors are obtained.

4 Model validation

Some experimental results available in the literature are used to validate the credibility of the two-phase model developed in ANSYS. The comparison is made for both single-phase and two-phase models. For the single-phase model, the cooling liquid in the microchannel is water. The microchannel consists of solid and fluid regions. Constant heat flux is applied at the bottom of the solid. The top of the channel is subjected to convective heat transfer,

while the adiabatic condition is applied to the remaining boundaries in the solid domain. Numerical results of the temperature difference and pressure drop are compared with the measured experimental results of Qu and Mudawar (2002) in Figs. 2, 3, respectively. The two-phase Eulerian–Eulerian model is compared with the experimental results of Kalteh et al. (2012)—alumina/water, and Li and Xuan (2002)—copper/water hybrid for the Nusselt number in Fig. 4. The two phases are allowed to enter the microchannel with the same axial velocity, and the exit condition is assumed for both phases. A good agreement is obtained between the numerical and experimental results. The error analyses used in the present study show that the average deviation (AD) and mean average deviation (MAD) calculated for the temperature difference and pressure drop are -2.661 and 2.661 and -2.383 and 11.004, respectively (Table 3). The formulae used to calculate the AD and MAD can be found in Eqs. (28) and (29).

5 Grid independence test

A Grid independence study is conducted using the base fluid (pure water) with a Reynolds number of 400 as the cooling liquid in the microchannel heat sink. The temperature difference between the channel inlet and outlet (ΔT) is monitored to test the grid independence of the different mesh element sizes, as shown in Table 4. Various mesh element sizes between 520,295 and 1,522,049 are considered for this test until the criterion of $\left| \frac{\Delta T_i - \Delta T_{i-1}}{\Delta T_i} \right| \leq 0.01$ was satisfied. Element size 1,365,109 is thus considered for this study.

6 Result and discussion

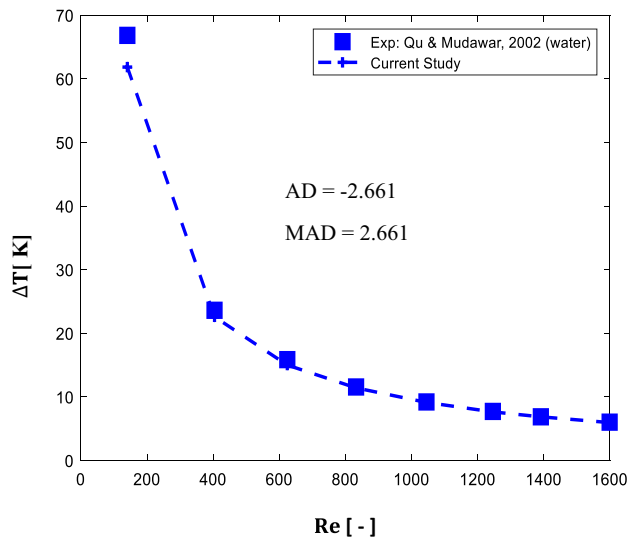
This section presents the results of the effects of nanoparticle hybridization on the substrate temperatures, thermal resistance, Nusselt number, pressure drop, FOM, and wall temperature. For the simulation study, the Reynolds number is varied between 400 and 1200, and the nanoparticle concentration ranges between zero (pure water) and 3.0% volume with different combinations of the particles.

6.1 Effect of hybridization of nanoparticles on the substrate temperature

The substrate temperature as a function of Reynolds number for different concentrations of the hybrid nanofluid and base fluid is presented in Fig. 5. The results show that the substrate temperature decreases with an increase in the Reynolds number. The following four mechanisms, among others,

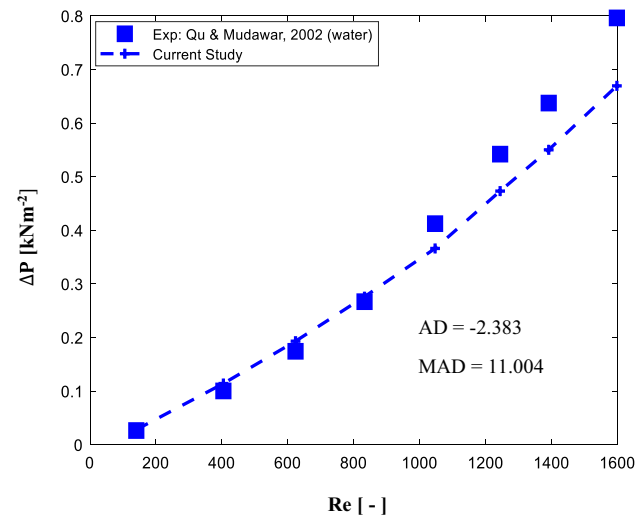
Table 3 The statistical analyses of the validated data

S/N		% Vol. composition	AD	MAD
Nusselt number				
1	Kalteh et al. (2012)	0.1% alumina	-0.812	0.812
2	Li and Xuan (2002)	1.5% Cu/water	-0.860	2.038
3	Li and Xuan (2002)	1.0% Cu/water	-0.604	1.193
Pressure drop				
4	Qu and Mudawar (2002)	Deionized water	-2.383	11.004
Temperature difference				
5	Qu and Mudawar (2002)	Deionized water	-2.661	2.661

**Fig. 2** Comparison of the present study for temperature difference with the experimental result of Qu and Mudawar (2002)

drive heat removal from the substrate: thermal conductivity, axial conduction and reduction in the thermal boundary layer, and the migration diffusion of the nanoparticles in the suspension. The predominant mechanism controls the ability of the hybrid nanofluid to remove heat from the substrate hence lowering its temperature.

This indicates why the nanofluids give lower substrate temperature compared with the base fluid. It is noted that there is a 3.0% to 6.0% reduction in the substrate temperature for $Re = 400$. Lower substrate temperatures are noted for nanofluids with a high concentration of copper nanoparticles. In addition, an increase in the composition of copper nanoparticles increases the thermal conductivity of the suspension and the ability to remove heat faster and more efficiently. This is possibly why the lowest temperature is obtained for hybrid nanofluid with the highest concentration of copper nanoparticles.

**Fig. 3** Comparison of the present study for pressure drop with the experimental result of Qu and Mudawar (2002)

6.2 Effect of nanoparticle hybridization on the thermal resistance

Figure 6 shows the significance of nanoparticle hybridization on the thermal resistance of the microchannel heat sink. Generally, as the Reynolds number increases, the resistance to heat flow from the heat source to the hybrid nanofluid decreases. The addition of nanoparticles reduces the thermal resistance due to the increase in the thermal conductivity and reduction of the thermal boundary layer etc. In their study, Kumar and Kumar (2020) reported this reduction in thermal resistance with increased nanofluid concentration. It has been shown that the increase in the concentration of copper nanoparticles increases the suspension's thermal conductivity, hence reducing the thermal resistance. A 34.0% reduction in the thermal resistance is observed for the 1.5% vol. (0.2% Al_2O_3 + 1.3% Cu) for $Re = 400$ and 41.0% for $Re = 1200$.

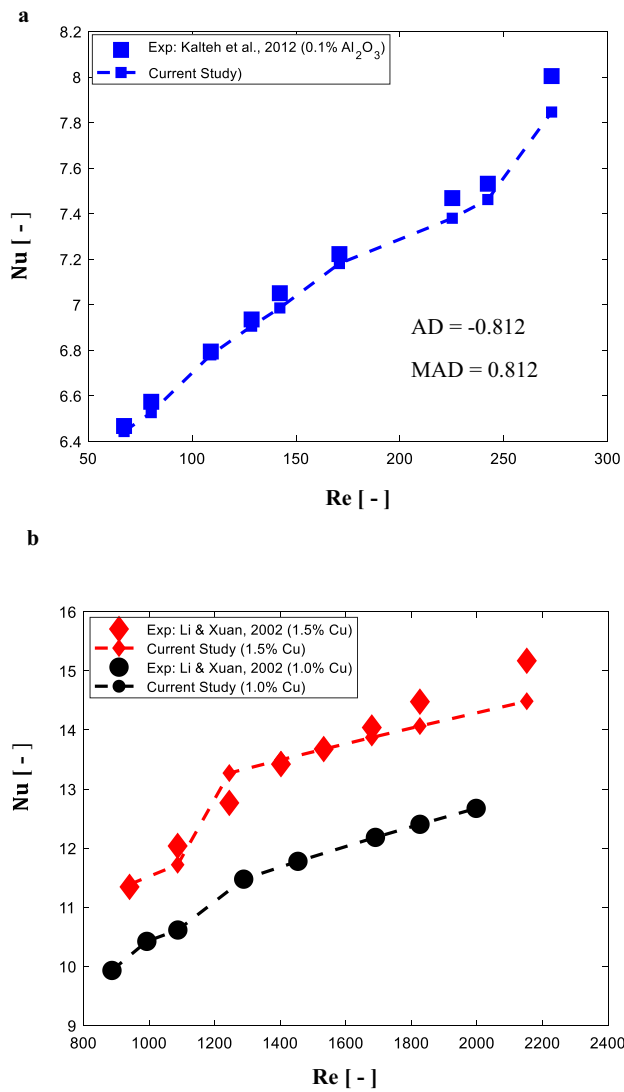


Fig. 4 Comparison of the present study for Nusselt number with the experimental result of **a** Kalleh et al. (2012), and **b** Li and Xuan (2002)

Table 4 Grid independent test

Mesh element	$\Delta T(k)$	$\frac{ \Delta T_i - \Delta T_{i-1} }{\Delta T_i}$
520,295	21.3179	–
880,088	22.6565	0.0591
1,073,654	23.4725	0.0348
1,365,109	23.6989	0.0095
1,522,049	23.8203	0.0051

6.3 Effect of nanoparticle hybridization on the average Nusselt number

The effect of hybridization on the Nusselt number is presented in Fig. 7. The result shows that the Nusselt number

only increases slightly with an increase in the Reynolds number. Ataei et al. (2020) and Kumar and Sarkar (2019, 2020), in their studies, obtained a more considerable increase in Nusselt number with an increase in Reynolds number. Hybrid nanofluids produce a higher Nusselt number relative to the base fluid. This can be attributed to the increased thermal conductivity, particle migration resulting from the Brownian diffusion, and the reduction in the thermal boundary layer. Also, an increase in the volume concentration of nanoparticles increases the nanofluid's inter-collision frequency, hence the thermal performance. However, nanofluid with a relatively high volume of concentration of Cu nanoparticles produces higher thermal performance due to the relatively higher thermal conductivity compared with alumina and the superiority of the thermal conductivity to the inter-collision frequency of the nanoparticles in the nanofluid. This can explain why the hybrid nanofluid with 1.5% vol. concentration though produces lower inter-collision frequency when compared with 3.0% vol. concentration but higher thermal performance.

The lowest Nusselt number is obtained for 0.5% vol., though it has a higher concentration of copper nanoparticles (0.3%) when compared with 0.2% vol. concentration in the 3.0% hybrid nanofluid. This can be due to the nanoparticles' lower average thermal conductivity and intercollision frequency.

6.4 Effect of nanoparticle hybridization on pressure drop

Figure 8 presents the effect of hybridization on the pressure drop. The result reveals that pressure drop is significantly

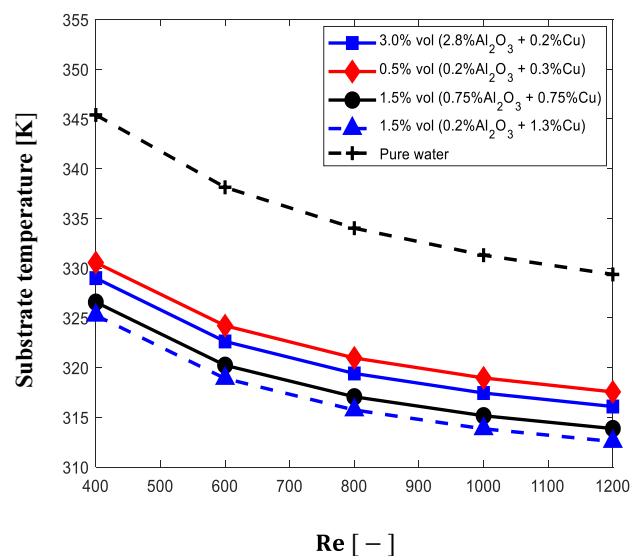


Fig. 5 Effect of hybridization of nanoparticles on the substrate temperature

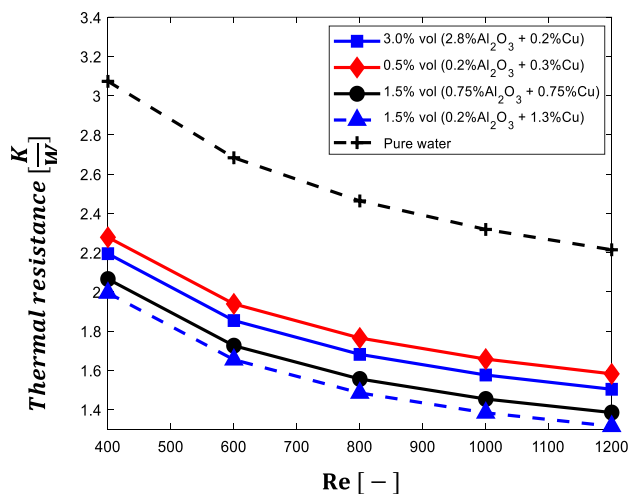


Fig. 6 Effect of nanoparticle hybridization on the thermal resistance of the microchannel heat sink

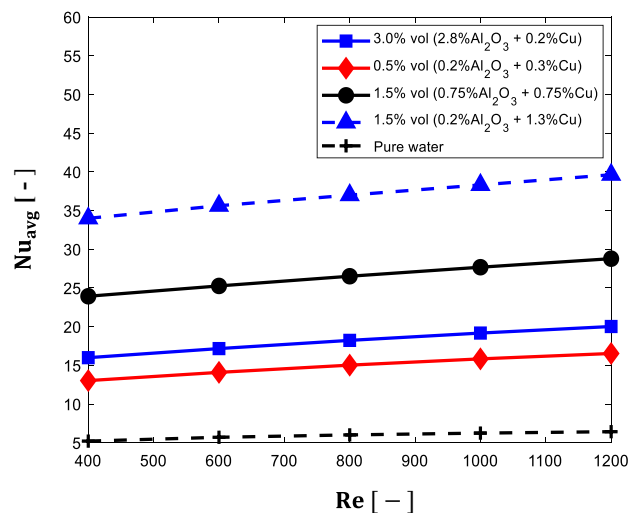


Fig. 7 Effect of nanoparticle hybridization on Nusselt number

increased by increasing Reynolds number but less influenced by the hybrid nanofluids relative to the base fluid. Irrespective of the volume concentration of the alumina-copper hybrid nanofluid, the concentration of the copper nanoparticles significantly affects the pressure drop. Though for Kumar and Sarkar (2019) increase in TiO_2 composition in the Al_2O_3/TiO_2 -water nanofluid does not significantly change the pressure drop due to the low particle volume fraction. $Al_2O_3/MWCNT$ -DI water nanofluid gave the highest pressure drop with an enhancement of about 22% compared to water (Kumar and Sarkar 2020), while Ataei et al. (2020) noted that Al_2O_3/TiO_2 -water reduced the pressure penalty compared with TiO_2 -water nanofluid. It has been shown that an increase in the composition/ concentration

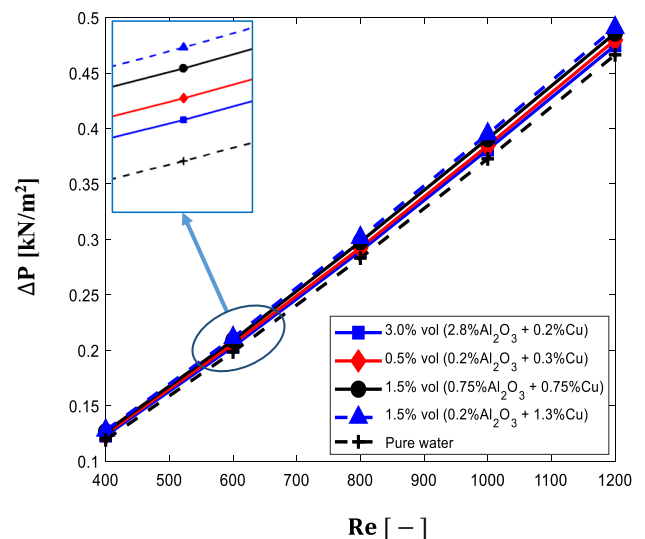


Fig. 8 Variation of pressure drop with Reynolds number. Arrows showing the magnified section in the oval shape

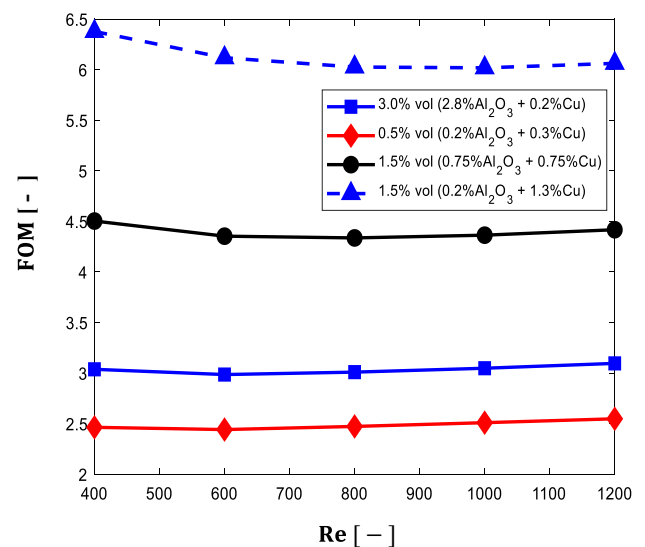


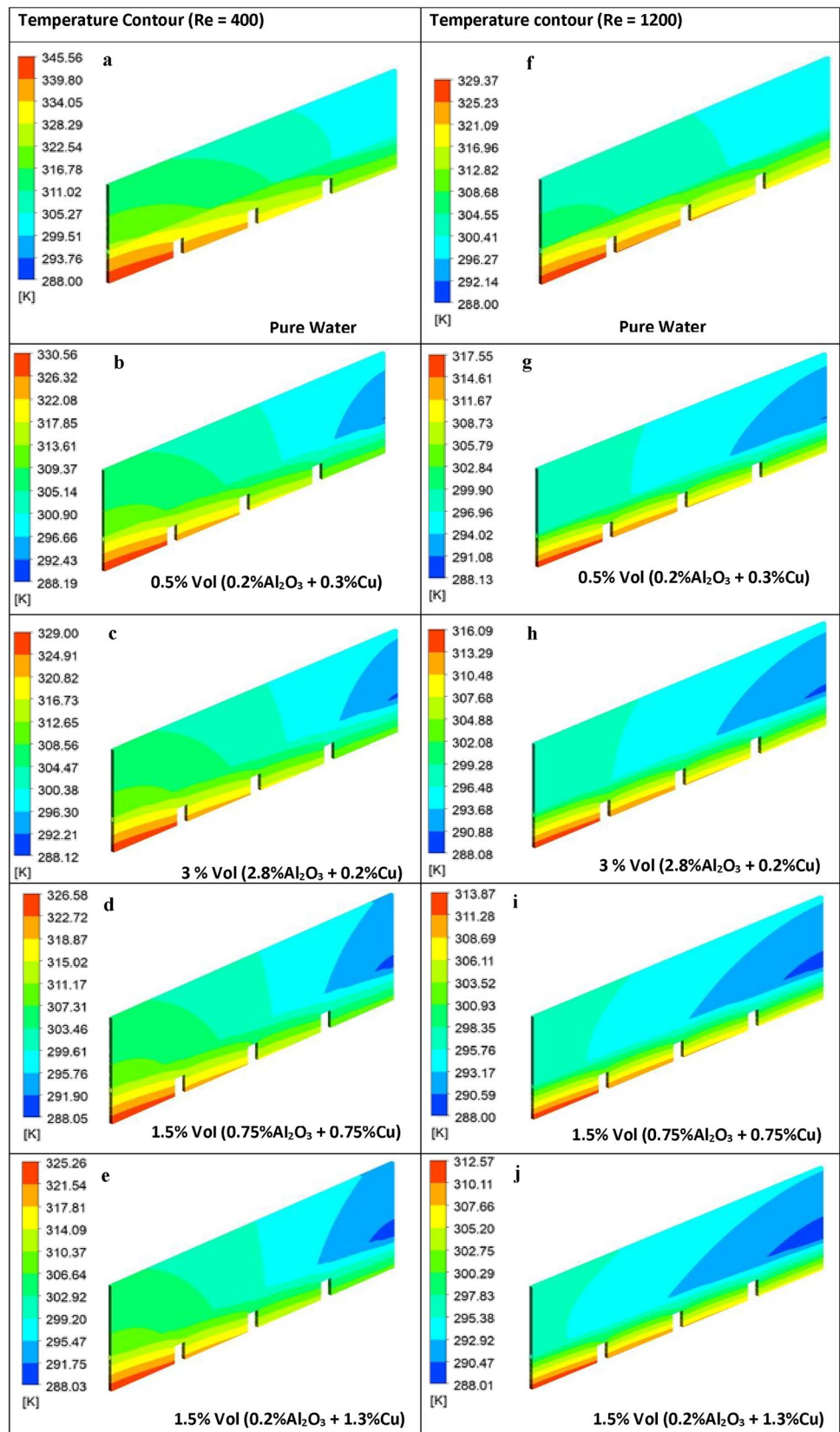
Fig. 9 Variation of performance evaluation criterion with Reynolds number

of copper nanoparticles in the present study increases the relative density and viscosity hence the pressure drop. An increase in the concentration of alumina seems to have a minimal effect on the pressure drop.

6.5 Effect of nanoparticle hybridization on the FOM

It is not enough to enhance the thermal performance or reduce the pressure penalty in a heat exchange system using nanofluid; it is essential to note how much gain in

Fig. 10 The wall temperature distribution contours of the microchannel with varying nanofluid particle concentration of between 0.5 and 3.0%



the thermal enhancement relative to the pressure drop. An additional benefit of the figure of merit (FOM) is that the optimal design and operating conditions can be evaluated.

For most heat transfer augmentation strategies, the heat transfer enhancement is always accompanied by an increased pressure drop. FOM compares the heat transfer increment with the pumping power or energy expended to drive the fluid, and $FOM > 1$ indicates that the thermal performance is greater than the energy used to move the fluid. For this reason, the method is accepted as a worthy solution technique for heat transfer augmentation (Kumar and Sarkar 2020).

$$FOM = \frac{h_{nf}/h_{bf}}{\left(p_{f,nf}/p_{f,bf}\right)^{\frac{1}{3}}} \quad (30)$$

where, h_{nf} , h_{bf} , $p_{f,nf}$ and $p_{f,bf}$ are the nanofluid and base fluid heat transfer coefficients, nanofluid, and base fluid frictional pressure drops.

Figure 9 reveals the effect of hybridization on FOM as the Reynolds number increases. The result shows that FOM increases with the average thermal conductivity of the hybridized nanofluid. The 3.0% vol. (2.8% vol. $Al_2O_3 + 0.2\%$ vol. Cu) has a higher effective thermal conductivity than the 0.5% vol. (0.2% vol. $Al_2O_3 + 0.3\%$ vol. Cu). Though the latter has a higher composition of copper nanoparticles than the former, the higher effective/ average thermal conductivity and rate of inter-collision resulting from the Brownian diffusion give the former a superior thermal performance. For 1.5% vol. concentration—high copper nanoparticle composition (0.75–1.3% vol.), the maximum FOM corresponds to Reynolds number of 400 while for lower copper concentration (<0.75% vol.) it is 1200. The least FOM corresponds to $Re = 600$ for Cu concentration lower than 0.75% vol. while $Re = 800$ is obtained for the concentration of Cu > 0.75% vol. However, Kumar and Sarkar (2020) noted a maximum FOM for some of the hybrid nanofluids investigated when the Reynolds number was 345; though, they considered alumina and the hybrid of alumina with other nanoparticles such as MgO, SiC, AlN, Cu, and CNT for flows with Reynolds number between 50 and 500.

6.6 Temperature variation contour in the microchannel wall

Figures 10 (a–f) represents the three-dimensional contour of the wall temperature distribution for Reynolds number of 400, and Figs. 10 (g–l) for Reynolds number of 1200 for different hybrid nanofluid concentrations. As shown in Fig. 10,

the wall temperature in the microchannel decreases as the concentration of copper particles in the hybrid nanofluid increase. This temperature decrease is more pronounced for the Reynolds number of 1200 due to an increase in the rate of heat transfer, the velocity of the bulk fluid, increased Brownian diffusion, and axial conduction.

7 Conclusions

A numerical study of the thermal performance and pressure of water-based alumina-copper hybrid nanofluid flowing through a narrow rectangular microchannel with a heat sink is considered. The numerical simulation was done using ANSYS Fluent, a computational fluid dynamics software. The effect of copper and alumina hybridization is investigated on the bulk temperature, substrate temperature, thermal resistance of the microchannel, Nusselt number, and pressure drop as a function of the Reynolds number. The Reynolds number varies between 400 and 1200, the volume concentration between 0.5 and 3.0%, and the concentration of alumina and copper in different proportions in the hybrid nanofluid for a constant heat flux of 1.0 MW/m^2 . The following are noted:

- (1) Increase in the concentration of copper nanoparticles in the hybridized nanofluid decreases the thermal resistance, substrate, and wall temperatures but increases the Nusselt number, pressure drop, and figure of merit.
- (2) For an effective design and operation of the heat exchange system, the FOM is an essential tool for evaluation. The maximum FOM corresponds to:
 - (a) Reynolds number of 400 for a high ($\geq 0.75\%$) copper nanoparticle concentration in the hybridized nanofluid.
 - (b) Reynolds number of 1200 for copper nanoparticle concentration less than 0.75%.

Acknowledgements This specific research did not receive any grant from funding agencies in the public, commercial, or not-for-profit sectors.

References

- Al Shdaifat MY, Zulkifli R, Sopian K, Salih AA (2020) Thermal and hydraulic performance of CuO/water nanofluids: a review. *Micromachines* 11:416. <https://doi.org/10.3390/mi11040416>
- Alihosseini Y, Targhi MZ, Heyhat MM, Ghorbani N (2020) Effect of a micro heat sink geometric design on thermo-hydraulic performance: a review. *Appl Therm Eng* 170:114974

- Ambreen T, Kim M (2017) Comparative assessment of numerical models for nanofluids' laminar forced convection in micro and minichannels. *Int J Heat Mass Transf* 115:513–523. <https://doi.org/10.1016/j.ijheatmasstransfer.2017.08.046>
- Ataei M, Moghanlou FS, Noorzadeh S, Vajdi M, Asl MS (2020) Heat transfer and flow characteristics of hybrid $\text{Al}_2\text{O}_3/\text{TiO}_2$ -water nanofluid in a minichannel heat sink. *Heat Mass Transf* 56(9):2757–2767
- Fard MH, Esfahany MN, Talaie MR (2010) Numerical study of convective heat transfer of nanofluids in a circular tube two-phase model versus single-phase model. *Int Commun Heat Mass Transf*. <https://doi.org/10.1016/j.icheatmasstransfer.2009.08.003>
- Ghasemi SE, Ranjbar AA, Hosseini MJ (2017) Numerical study on effect of CuO-water nanofluid on cooling performance of two different cross-sectional heat sinks. *Adv Powder Technol*. <https://doi.org/10.1016/j.apt.2017.03.019>
- Gunn DJ (1978) Transfer of heat or mass to particles in fixed and fluidised beds. *Int J Heat Mass Transf* 21(4):467–476. [https://doi.org/10.1016/0017-9310\(78\)90080-7](https://doi.org/10.1016/0017-9310(78)90080-7)
- Kalteh M, Abbassi A, Saffar-Avval M, Harting J (2011) Eulerian-Eulerian two-phase numerical simulation of nanofluid laminar forced convection in a microchannel. *Int J Heat Fluid Flow* 32(1):107–116. <https://doi.org/10.1016/j.ijheatfluidflow.2010.08.001>
- Kalteh M, Abbassi A, Saffar-Avval M, Frijns A, Darhuber A, Harting J (2012) Experimental and numerical investigation of nanofluid forced convection inside a wide microchannel heat sink. *Appl Therm Eng* 36(1):260–268. <https://doi.org/10.1016/j.applthermaleng.2011.10.023>
- Kumar PCM, Kumar CMA (2020) Numerical study on heat transfer performance using Al_2O_3 /water nanofluids in six circular channel heat sink for electronic chip. *Mater Today Proc* 21:194–201. <https://doi.org/10.1016/j.matpr.2019.04.220>
- Kumar V, Sarkar J (2019) Numerical and experimental investigations on heat transfer and pressure drop characteristics of Al_2O_3 - TiO_2 hybrid nanofluid in minichannel heat Sink with different mixture ratio. *Powder Technol* 345:717–727. <https://doi.org/10.1016/j.apt.2019.11.017>
- Kumar V, Sarkar J (2020) Experimental hydrothermal characteristics of minichannel heat sink using various types of hybrid nanofluids. *Adv Powder Technol* 31(2):621–631. <https://doi.org/10.1016/j.apt.2019.11.017>
- Labib MN, Nine MJ, Afrianto H, Chung H, Jeong H (2013) Numerical investigation on effect of base fluids and hybrid nanofluid in forced convective heat transfer. *Int J Therm Sci*. <https://doi.org/10.1016/j.jthermalsci.2013.04.003>
- Li Q, Xuan Y (2002) Convective heat transfer and flow characteristics of Cu-water nanofluid. *Sci China, Ser E Technol Sci* 45(4):408–416. <https://doi.org/10.1360/02ye9047>
- Madalina G, Huminic G, Adriana A, Huminic A (2018) Experimental study on thermal conductivity of stabilized Al_2O_3 and SiO_2 nanofluids and their hybrid. *Int J Heat Mass Transf* 127:450–457. <https://doi.org/10.1016/j.ijheatmasstransfer.2018.07.024>
- Madhesh D, Parameshwaran R, Kalaiselvam S (2014) Experimental investigation on convective heat transfer and rheological characteristics of Cu- TiO_2 hybrid nanofluids. *Exp Therm Fluid Sci*. <https://doi.org/10.1016/j.expthermflusci.2013.08.026>
- Minea AA (2020) Pumping power and heat transfer efficiency evaluation on Al_2O_3 , TiO_2 and SiO_2 single and hybrid water-based nanofluids for energy application. *J Therm Anal Calorim* 139(2):1171–1181. <https://doi.org/10.1007/s10973-019-08510-3>
- Nimmagadda R, Venkatasubbaiah K (2017) Two-phase analysis on the conjugate heat transfer performance of microchannel with Cu, Al, SWCNT, and hybrid nanofluids. *J Therm Sci Eng Appl*. <https://doi.org/10.1115/1.4036804>
- Pinto RV, Fiorelli FAS (2016) Review of the mechanisms responsible for heat transfer enhancement using nanofluids. *Appl Therm Eng*. <https://doi.org/10.1016/j.applthermaleng.2016.07.147>
- Qu W, Mudawar I (2002) Experimental and numerical study of pressure drop and heat transfer in a single-phase micro-channel heat sink. *Int J Heat Mass Transf* 45(12):2549–2565. [https://doi.org/10.1016/S0017-9310\(01\)00337-4](https://doi.org/10.1016/S0017-9310(01)00337-4)
- Rajiv KH, Sokhal GS (2020) Effect of geometries and nanofluids on heat transfer and pressure drop in microchannels: a review. *Mater Today: Proc* 28(3):1841–1846
- Rowe PN (1961) Drag forces in a hydraulic model of a fluidized bed-Part II. *Trans Inst Chem* 39:175–180
- Sarkar JA (2011) critical review on convective heat transfer correlations of nanofluids. *Renew Sust Eng Rev*. <https://doi.org/10.1016/j.rser.2011.04.025>
- Selvakumar P, Suresh S (2012) Use of Al_2O_3 -Cu/water hybrid nanofluid in an electronic heat sink. *IEEE Trans Compon, Packag Manuf Technol*. <https://doi.org/10.1109/TCPMT.2012.2211018>
- Shkarah AJ, Bin Sulaiman MY, Ayob MRBH, Togun H (2013) A 3D numerical study of heat transfer in a single-phase micro-channel heat sink using graphene, aluminum and silicon as substrates. *Int Commun Heat Mass Transf* 48:108–115. <https://doi.org/10.1016/j.icheatmasstransfer.2013.08.006>
- Snoussi L, Ouerfelli N, Sharma KV, Vranceanu N, Chamkha AJ, Guizani A (2018) Numerical simulation of nanofluids for improved cooling efficiency in a 3D copper microchannel heat sink (MCHS). *Phys Chem Liq* 56(3):311–331. <https://doi.org/10.1080/00319104.2017.1336237>
- Suresh S, Venkataraj KP, Selvakumar P, Chandrasekar M (2012) Effect of Al_2O_3 -Cu/water hybrid nanofluid in heat transfer. *Exp Therm Fluid Sci*. <https://doi.org/10.1016/j.expthermflusci.2011.11.007>
- Suresh S, Venkataraj KP, Selvakumar P (2011) Synthesis, characterisation of Al_2O_3 -Cu nano composite powder and water based nanofluids. *Adv Mat Res*. <https://doi.org/10.4028/www.scientific.net/AMR.328-330.1560>
- Wen CY, Yu YH (1966) Mechanics of fluidization. *Chem Eng Prog Symp Series* 62:100–111
- Yildizeli A, Cadirci S (2020) Multi objective optimization of a micro-channel heat sink through genetic algorithm. *Int J Heat Mass Transf*. <https://doi.org/10.1016/j.ijheatmasstransfer.2019.118847>

Publisher's Note Springer Nature remains neutral with regard to jurisdictional claims in published maps and institutional affiliations.

Authors and Affiliations

Oluwasegun S. Omosehin¹ · Adekunle O. Adelaja¹  · Olabode T. Olakoyejo¹ · Manasseh O. Oyekeye¹

✉ Adekunle O. Adelaja
aadelaja@unilag.edu.ng

¹ Department of Mechanical Engineering, University of Lagos, Akoka, Yaba, Lagos 101017, Nigeria